J Mater Sci: Mater Electron (2021) 32:8798–8806

Dielectric measurements on stearic acid/eicosylamine alternate layer Langmuir–Blodgett films incorporating CdS nanoparticles

R. Capan[1,*] and A. K. Ray[2]

[1] Science Faculty, Physics Department, Balikesir University, 10100 Balikesir, Turkey
[2] Institute of Materials and Manufacturing, Brunel University London, Uxbridge UB8 3PH, Middlesex, UK

Received: 31 December 2020
Accepted: 12 February 2021
Published online: 30 March 2021

ABSTRACT

Langmuir–Blodgett deposition of 16 and 15 monolayers of stearic acid/eicosylamine has been accomplished on ultrasonically cleaned aluminized quartz substrate with 50 nm thick evaporated aluminium electrodes. Alternating current (AC) impedance measurements have been performed on with the aluminium (Al) top electrode in a sandwich configuration in the range of 100 Hz to 1 MHz and in the temperature ranging between 300 K $\leq T \leq$ 360 K. The impedance data were fitted using an equivalent circuit which is mainly composed of resistors and constant phase elements (CPE). Complex impedance study highlighted the presence of a non-Debye type relaxation conduction: quantum mechanical tunnelling (QMT) through the barrier separating the localized sites and correlated barrier hopping.

1 Introduction

The Langmuir–Blodgett (LB) technique is to deposit highly defined structured, and nanometre scale thick films by transferring the floating layer of amphiphilic molecules from the air–water interface to the surface of a solid substrate [1]. Uniform deposition of LB films, with molecular thickness over a comparatively large area can be exploited for large-area electronics. Different types of LB insulating layers of fatty acids, long-chain diacetylene on inorganic semiconducting substrates have been used as dielectric layer for fabricating reasonably stable field-effect transistors [2]. In recent years, a range of biosensors using LB films has been reported for development of reasonably sensitive biosensors for clinical applications involving dengue NS1 antigen, NADH, HUVEC and Glucose with encouraging detection limits and repeatability. The incorporation of metal nanocrystals (NC) such as CuS, PbS, ZnS, CdS, CdZnS and ZnO into LB films has stimulated the investigation for interesting applications for photodetectors, electroluminescence emitters as active media [3]. The CdS sizes increase with the number of LB monolayer about 10–100% with increasing the in the initial matrix from 3 to 20 ML [4]. Also polarized preferential orientation of molecules in the LB film structure manipulate organic materials at the molecular

Address correspondence to E-mail: rcapan@balikesir.edu.tr

https://doi.org/10.1007/s10854-021-05551-z

level and to fabricate devices consisting of a layered Metal/LB film/Metal (M/LB/M) structure, suitable for pyroelectric and electronic applications [5].

In our previous work, the bilayer thickness for the LB films was estimated to be 4.65 nm without CdS and 5.28 nm with CdS nanoparticles, respectively [6]. The active area S of the device is found to be 4×10^{-6} m^2. The details of the preparation of the Al/Al_2O_3/LB film/Al device structures are available from our earlier publications [7].

In this work, the frequency response of the conductivity and capacitance of sandwiched between two aluminium (Al) electrodes is investigated by applying an AC signal with the amplitude of 0.1 V and sweeping frequency from 100 Hz to 1 MHz at temperatures ranging from 300 to 360 K. This non-destructive impedance spectroscopy, measuring the AC electrical response over a wide frequency range between 100 Hz and 1 MHz, can predict the conductivity, structural homogeneity and stability considering the relative contributions of grain, grain boundary and defect states in thin-film materials. Impedance spectroscopy is a simple analytical tool to determine electrical conductivity through various parameters like complex impedance complex electric modulus, complex dielectric permittivity [8, 9].

2 Experimental details

A NIMA 622 type Langmuir–Blodgett (LB) trough was used to deposit a non-centrosymmetric alternate layer LB film structure on an ultrasonically cleaned aluminized quartz substrate. As shown in Fig. 1, LB film consists of stearic acid [$CH_3(CH_2)_{16}CO_2H$] and eicosylamine [$CH_3(CH_2)_{19}NH_2$], 16 and 15 monolayers, respectively, sandwiched between two 50 nm thick thermally deposited aluminium electrodes. In order to incorporate cadmium sulphide (CdS) nanoparticles in the LB film, the cadmium chloride ($CdCl_2$) was dissolved in the water subphase to a concentration of approximately 0.5×10^{-4} M. Further information on the LB deposition of a non-centrosymmetric alternate layer can be found from one of our previous publication [6]. The conductivity as a function of frequency f ranging from 20 Hz to 1 MHz using a Hewlett Packard 4284 LCR meter and Oxford instrument constant bath cryostat in a microprocessor-controlled measuring system over a temperature (T) range of 300–360 K. During the entire measurements, the temperature was recorded with the stability lying with the region of ± 0.5 K. The samples were kept under vacuum before testing to avoid any thermal current problems due to absorbed moisture and trapped charge collected from the air. An electrical equivalent circuit for the Al/Al_2O_3/LB film/Al sandwich structure is given in Fig. 2. In this diagram, R_B and R_T are the resistance of the bottom and top aluminium electrodes, R_O and C_O are the resistance and capacitance of the oxide layer, and R_{LB} and C_{LB} are the resistance and capacitance of the LB film multilayer.

3 Result and discussion

Experimental results were presented for dielectric relaxation in Al/Al_2O_3/LB film/Al film structures along with the evaluation of values of relevant physical parameters.

Figure 3 shows the variation in AC capacitance, C_{ac} and conductance σ_{ac} with frequency f within the range of $20\,\text{Hz} \geq f \geq 10^6\,\text{Hz}$ at temperatures T varying between 300 and 360 K for Al/Al_2O_3/LB film/Al structure. It compares capacitance and conductance measurements as a function of $\log f$ for the alternate layer LB film with and without CdS nanoparticles at the temperature range $300\,\text{K} \leq T \leq 360\,\text{K}$. Capacitance results for both LB film samples show small decrease initially up to $f = 100\,\text{kHz}$ and then a sharp reduction with increasing frequency. The behaviour pattern for conductance is, on the other hand, opposite. The capacitance values decrease with increasing temperatures for both samples. Figure 3c presents the capacitance and conductance behaviours as a function of $\log f$ at room temperature of 300 K. The results showed that the capacitance value of CdS nanoparticle is higher than the capacitance value of without CdS nanoparticles. Conductance of CdS nanoparticle is lower than without CdS nanoparticles. Conductance measurements indicate a small increase until 100 kHz and a sharp increase is occurred. Both structures showed characteristically similar behaviour. Two different regions are found to exist in Fig. 3c, depending upon the frequency range. The plateau of AC conductivity (σ_{ac}) for the lower frequency range ($f \leq 10\,\text{kHz}$) corresponds to the frequency independent DC conductivity (σ_{dc}) [10]. The frequency dependence of conductivity or so-called universal dynamic response

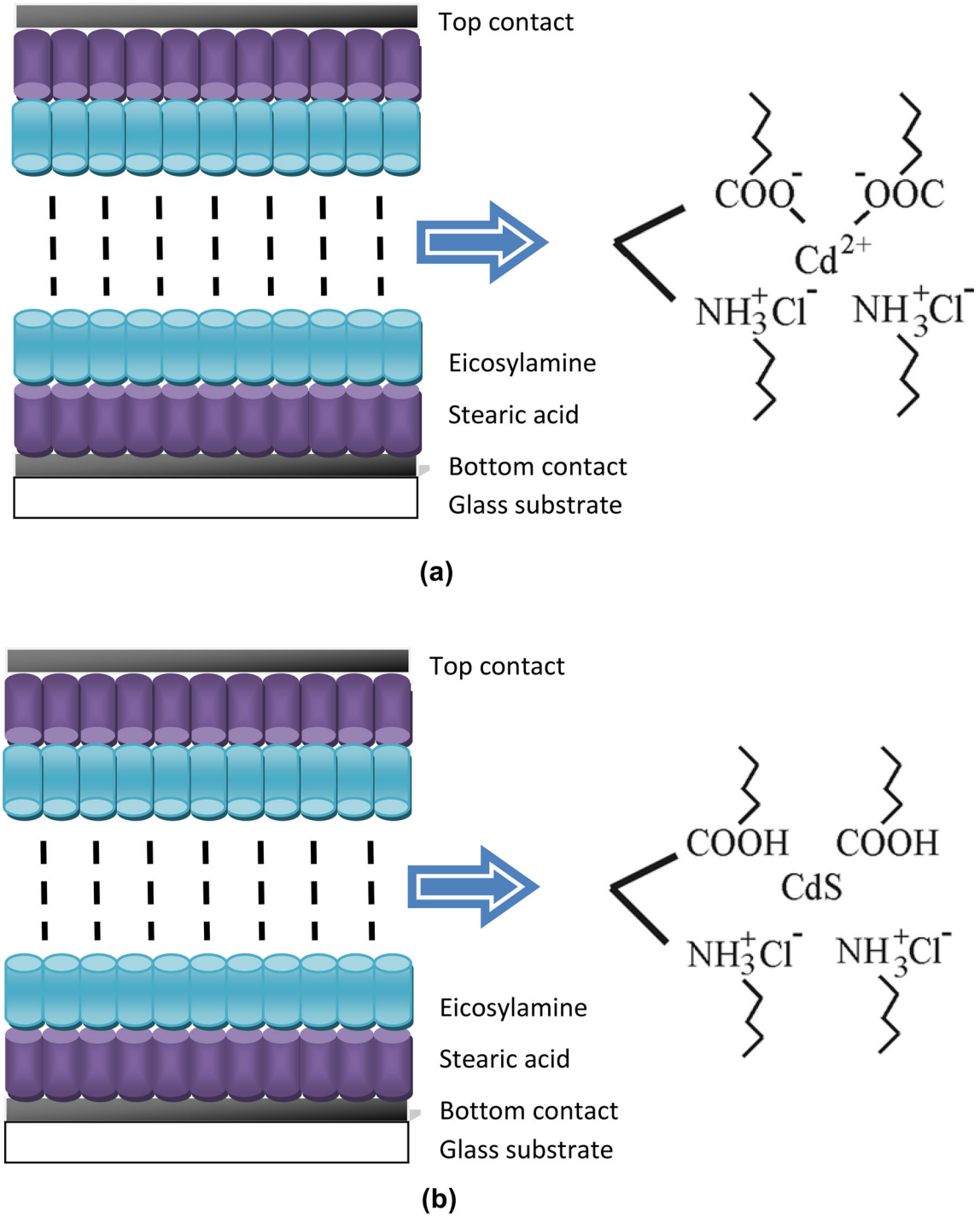

Fig. 1 A schematic diagram of stearic acid/eicosylamine LB film **a** before H_2S exposure, **b** after H_2S exposure

(UDR) of ionic conductivity is related by a simple expression given by Jonscher's power law [11]. The (ω, T) over wide range of frequency and temperature can be represented by the UDR relation [12].

At the higher frequency, the AC conductivity (σ_{ac}) increases in parallel with the increase in frequency and obeying to power law $\sigma_{ac} \propto \omega^s$ and the increase in conductivity is due to the hopping of charge carrier in the film structure.

Electrical conductivity of solid electrolytes as a function of frequency can generally be described as frequency independent, dc conductivity σ_{dc}, and a

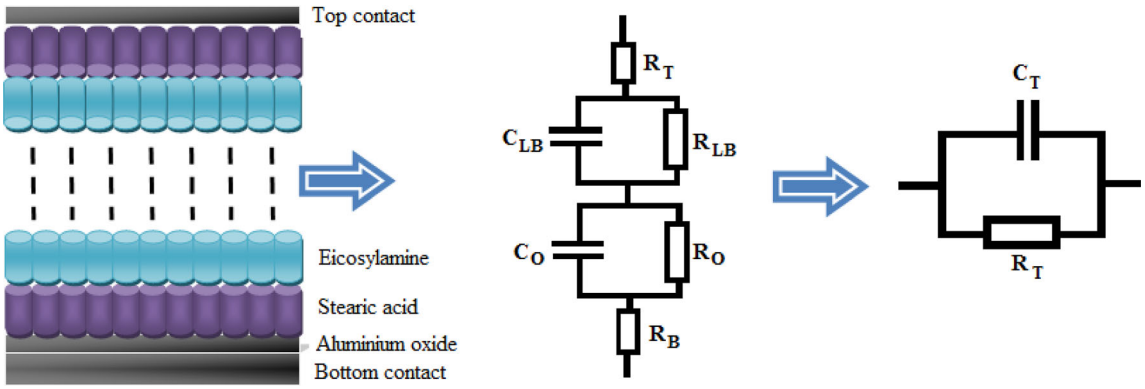

Fig. 2 Equivalent circuit for the $Al/Al_2O_3/$, LB film/Al sandwich structure

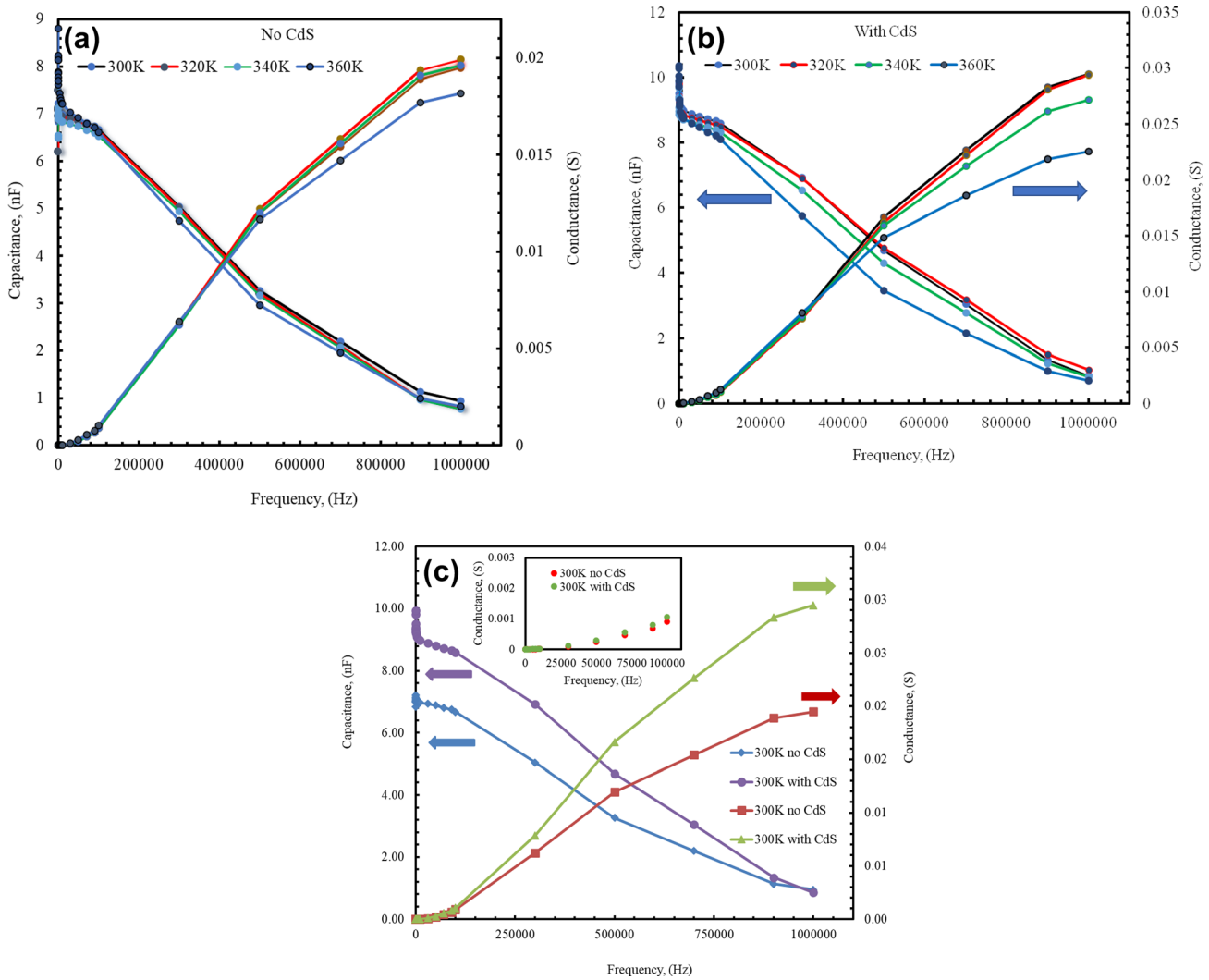

Fig. 3 Capacitance and conductance as a function of frequency **a** no CdS, **b** with CdS, **c** comparing at 300 K. The inset is the conductance response versus frequency between 1 and 10^5 Hz

strongly frequency dependent components. A typical frequency dependence of conductivity spectrum exhibits three distinct regions (a) low-frequency dispersion (b) an intermediate frequency plateau and (c)

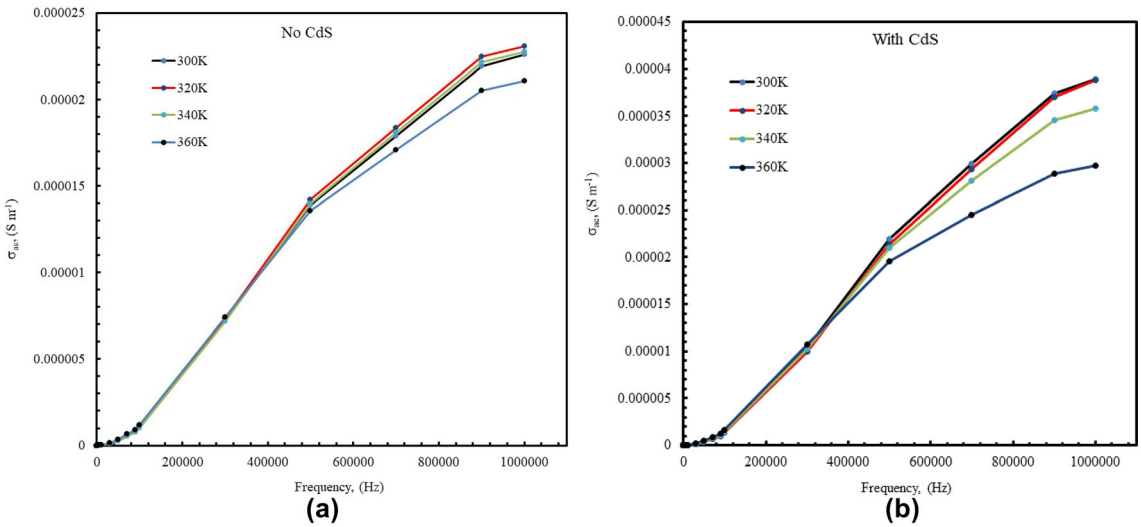

Fig. 4 Frequency dependence of AC conductivity **a** no CdS, **b** with CdS

Table 1 Values of s and W_M at several temperatures

Temperature (K)	s value for no CdS	s value for CdS	W_M for no CdS (eV)	W_M for CdS (eV)
300	0.729	0.848	0.572	1.020
310	0.723	0.870	0.559	1.192
320	0.727	0.882	0.568	1.314
330	0.728	0.882	0.570	1.314
340	0.732	0.790	0.578	0.738
350	0.691	0.753	0.501	0.627
360	0.659	0.619	0.454	0.406

an extended dispersion at high frequency [13]. The variation of conductivity in the low-frequency region is attributed to the polarization effects at the electrode and thin-film interface. As the frequency reduces, charge accumulation occurs in increasing amount at the electrode and thin-film interface, resulting a drop in conductivity. In the intermediate frequency plateau region, conductivity is almost found to be frequency independent and is equal to dc conductivity σ_{dc}. In the high-frequency region, the conductivity increases with the frequency. Using Jonscher's power law and the UDR relation, the $\sigma(\omega, T)$ can be represented as [11, 12]:

$$\sigma(\omega, T) = \sigma_{dc}(T) + \sigma_{ac}(\omega, T) \quad (1)$$

where σ_{dc} is the frequency-independent (electronic or DC) part of AC conductivity. The term $\sigma_{ac}(\omega, T) = A\omega^s$ can often be explained on the basis of two distinct mechanisms for carrier conduction: quantum mechanical tunnelling (QMT) through the barrier separating the localized sites and correlated barrier hopping (CBH) over the same barrier [14] s ($0 \leq s \leq 1$) is the index, $\omega = 2\pi f$ is angular frequency of applied AC field and A is $\left[A = \frac{\pi N^2 e^2}{6 k_B T 2\alpha}\right]$ [14] is a constant depending on temperature, e is the electronic charge, T is the temperature, α is the polarizability of a pair of sites, and N is the number of sites per unit volume among which hopping takes place. Such a variation is associated with displacement of carriers which move within the sample by discrete hops of length R between randomly distributed localized sites. The value of s has a physical significance. When s is less than or equal to 1, the hopping conduction engages a translational motion with a sudden hopping [15].

Figure 4 presents a set of reproducible curves on double logarithmic scales showing the frequency dependence of AC conductivity $\sigma_{ac}(\omega, T)$ of LB samples within the temperature range of 300 and 360 K. It is clear that the σ_{ac} remains almost constant at low frequency and after a certain frequency; it increases with power law with increasing frequency. Using $\sigma_{ac}(\omega, T) = A\omega^s$ where A is a constant of

proportionality [16] to a power law above 100 kHz the value of the exponent frequency, s, for various temperature has been determined from the linear slope of [log (ω, T)] versus [log ω]. We found that the calculated values of s decrease from 300 to 360 K. This behaviour can be explained in terms of correlated barrier hopping (CBH) model [17]:

$$\sigma_{ac}(\omega, T) = \frac{\pi^2 N^2 \varepsilon}{24}\left(\frac{8e^2}{\varepsilon W_M}\right)^6 \frac{\omega^s}{\tau_0^{1-s}} \quad (2)$$

where ε is the dielectric constant, e is the electronic charge and τ_0 is the characteristic relaxation time, which is in the order of atom vibrational period 10^{-13} s, W_M is the effective barrier height over which the electrons hopping energy gap between valence band and conduction band. Exponent s is evaluated as [18]:

$$s = 1 - \frac{6k_BT}{W_M - k_BT\ln\left(\frac{1}{\omega\tau_0}\right)} \quad (3)$$

For large values of $\frac{W_M}{k_BT}$, the exponent s can be given by [19]:

$$s = 1 - \frac{6k_BT}{W_M} \quad (4)$$

The behaviour of the exponent factor s as a function of temperature can be used to determine the origin of the conduction mechanism. Values of the frequency exponent s at different temperature were calculated from the slopes of linear part of the relation of log (ω, T) versus log ω at the higher-frequency range. Values of W_M are calculated from Eq. (4) and given in Table 1. It is observed that the frequency exponent s decreases with increasing temperature. Such behaviour suggests that the correlated barrier hopping (CBH) conduction mechanism is the predominant conduction mechanism. In CBH model, the conduction occurs via single polaron or bipolaron hopping process over the Coulomb barrier separating two defect centres [20]. As is known, a decrease of s with increasing temperature and convergence to one at low temperatures and high frequencies is the characteristic features of CBH model. According to CBH model, charge carriers hop between sites over the potential barrier, W_M, separating them [21].

The effective barrier height W_M decreases with increasing temperature which corresponds to the decrease in the exponent s. Therefore, the number of free carriers which can hop over the barrier will be

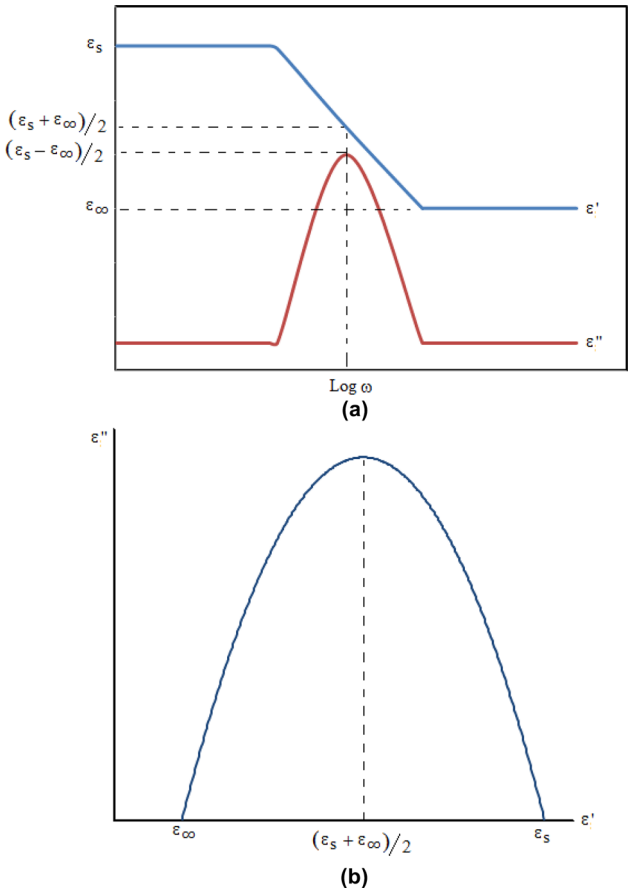

Fig. 5 Schematic representation of **a** Debye equations, **b** Cole–Cole plotted as a function of log ω

increased. Consequently, this behaviour confirms that the conduction process is a thermally activated process as shown the σ_{ac} increases with the increasing temperature. The value of W_M is equal or less than energy gap. This is due to the structure characteristics of the material such as the average grain size, orientation, defect distribution, phase content, and charge carrier density. All these factors were not taken into account in CBH model [12].

The dielectric relaxation equations (Debye or Cole–Cole) and its derivatives were used for analysis of the experimental permittivity data of stearic acid/eicosylamine alternate layer Langmuir–Blodgett films incorporating CdS nanoparticles over the frequency up to 1 MHz and temperature range of 300–360 K. The plots of dielectric constant ε' and loss factor ε'' against the frequency were found useful in determining how well experimental data fits the Debye or Cole–Cole equations [22, 23]. Equations (5) and (6) are known as Debye equations and they describe the

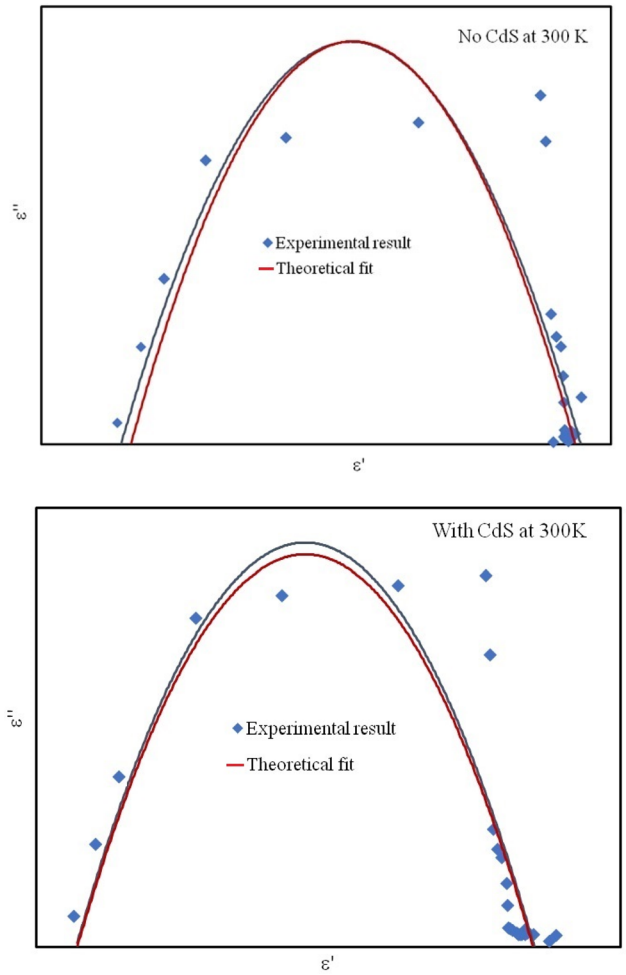

Fig. 6 Cole–Cole plot of dispersion curve of the stearic acid/eicosylamine LB films at 300 K

behaviour of polar dielectrics at various frequencies [24].

$$\varepsilon' = \varepsilon_\infty + \frac{\varepsilon_s - \varepsilon_\infty}{1 + \omega^2\tau^2} \tag{5}$$

$$\varepsilon'' = \frac{(\varepsilon_s - \varepsilon_\infty)\omega\tau}{1 + \omega^2\tau^2} \tag{6}$$

(1) For small values of $\omega\tau$, the real part $\varepsilon' \approx \varepsilon_s$ because of the squared term in the denominator of Eq. (5) and ε'' is also small for the same reason. Of course, at $\omega\tau = 0$, we get $\varepsilon'' = 0$ as expected because this is dc voltage
(2) For very large values of $\omega\tau$, $\varepsilon' = \varepsilon_\infty$ and ε'' is small
(3) For intermediate values of frequencies, ε'' is a maximum at some particular value of $\omega\tau$

The maximum value of ε'' is obtained at a frequency given by $\omega_p\tau = 1$ where ω_p is the frequency at $\varepsilon''_{\max}$.

Using Eqs. (5) and (6), the values of ε' and ε'' at this value of $\omega\tau$ are given as follows:

$$\varepsilon' = \frac{\varepsilon_s + \varepsilon_\infty}{2} \tag{7}$$

$$\varepsilon'' = \frac{\varepsilon_s - \varepsilon_\infty}{2} \tag{8}$$

The Debye relaxation model has been widely used in describing the way the molecules respond to the applied field and it is originally used with dipoles (molecules) that can be rotated in viscous liquid solutions. Therefore, this simple theory cannot be used to explain other viscous relaxation processes. A modification to the model has to be made to fit the experimental data to the theory that one of the suggestions proposed for LB films is the Cole–Cole dielectric relaxation model, which is given by [22]

$$\varepsilon = \varepsilon_\infty + \frac{\varepsilon_s - \varepsilon_\infty}{1 + (j\omega\tau)^\alpha} \tag{9}$$

where τ is the characteristic time at which cross-over from dynamical to statistical regime takes place. α $(0 < \alpha \leq 1)$ is a parameter added to specify the breadth of the experimental relaxation peaks. In

Table 2 Values of Cole–Cole plot at several temperatures

Temperature (K)	ε_s		ε_∞		$\frac{\varepsilon_s + \varepsilon_\infty}{2}$		$\varepsilon_s - \varepsilon_\infty$	
	No CdS	With CdS	No CdS	With CdS	No CdS	With CdS	No CdS	With CdS
300	3.77	4.25	0.35	0.58	2.06	2.42	3.42	3.67
310	3.76	4.20	0.60	0.60	2.18	2.40	3.16	3.60
320	3.80	4.25	0.80	1.00	2.30	2.62	3.00	3.25
330	3.80	4.20	0.95	1.10	2.38	2.65	2.85	3.10
340	3.80	4.15	0.60	1.10	2.20	2.63	3.20	3.05
350	4.10	4.10	0.50	1.00	2.30	2.55	3.60	3.00
360	4.35	4.30	0.50	0.50	2.43	2.40	3.85	3.80

order to determine which dielectric relaxation model is best for a particular experimental result, a Cole–Cole diagram is plotted. A Cole–Cole diagram is a plot of the imaginary permittivity ε'' against the real permittivity ε'. According to Debye theory, the Cole–Cole plot is a semicircle and according to Cole–Cole theory the plot is a skewed arc.

$$\left(\varepsilon' - \frac{\varepsilon_s - \varepsilon_\infty}{2}\right)^2 + \varepsilon''^2 = \left(\frac{\varepsilon_s - \varepsilon_\infty}{2}\right)^2 \quad (10)$$

where ε_s is the static, ε_∞ is induced permittivity of the material, $\left(\frac{\varepsilon_s - \varepsilon_\infty}{2}\right)$ is the radius and $\left(\frac{\varepsilon_s + \varepsilon_\infty}{2}, 0\right)$ is the coordinate of the centre of the semi-circle. The schematic diagram of the plot is given in Fig. 5.

The Cole–Cole plot of dispersion curve of the stearic acid/eicosylamine LB films obtained at 300 K is shown in Fig. 6. The plot is curve fitted so that the values of ε_s and ε_∞ can be estimated by extrapolating the values obtained to frequencies $\omega = 0$ and $\omega = \infty$, respectively. Similar calculations for ε_s and ε_∞ are made at different temperatures, and the values are given in Table 2. Static permittivity of relaxation, ε_s, for stearic acid/eicosylamine alternate layer LB film without CdS nanoparticles increases as the temperature increases. However, ε_s for stearic acid/eicosylamine alternate layer LB film incorporating CdS nanoparticles is almost the same. This could be attributed to the presence of the nanoparticles formed between the monolayers. It is believed that formation of these nanoparticles modifies layer-by-layer film order. If we assume that formation of the nanoparticles in the interface mainly modifies the film thickness but causes a little effect on ε_s as a function of temperature.

4 Conclusions

31 monolayers of stearic acid/eicosylamine with and without CdS nanoparticles LB film is fabricated for AC impedance measurements in the range of 100 Hz to 1 MHz using the temperature ranging between 300 K $\leq T \leq$ 360 K. Cole–Cole dielectric relaxation model is used to study dielectric relaxation properties of these LB films. The ε_s for stearic acid/eicosylamine alternate layer LB film incorporating CdS nanoparticles is higher than the ε_s for stearic acid/eicosylamine alternate layer LB film without CdS nanoparticles. The difference between ε_s and ε_∞ is the reflected by the diameter of Cole–Cole plot semicircle which corresponds to the orientation polarization that is related to the rotation of dipole molecules in the AC filed. The result appears that $\varepsilon_s - \varepsilon_\infty$ (given in Table 2) is changing between 3.42 and 3.85 for stearic acid/eicosylamine alternate layer LB film without CdS, between 3.67 and 3.80 for stearic acid/eicosylamine alternate layer LB film incorporating CdS nanoparticles with the temperature.

References

1. M.C. Petty, *Langmuir–Blodgett Films: An Introduction* (Cambridge University Press, Cambridge, 1996).
2. M.C. Petty, Thin Solid Films (1992). https://doi.org/10.1016/0040-6090(92)90300-Z
3. S.A. Batsanov, A.K. Gutakovskii, Nanotechnol. Russ. (2017). https://doi.org/10.1134/S1995078017040061
4. D.Y. Protasov, W.B. Jian, K.A. Svit, T.A. Duda, S.A. Teys, A.S. Kozhuhov, L.L. Sveshnikova, K.S. Zhuravlev, J. Phys. Chem. C (2011). https://doi.org/10.1021/jp206816f
5. S.A. Hussain, B. Dey, D. Bhattacharjee, N. Mehta, Heliyon (2018). https://doi.org/10.1016/j.heliyon.2018.e01038
6. R. Capan, A.K. Hassan, A.V. Nabok, A.K. Ray, T.H. Richardson, M.C. Simmonds, C. Sammon, IEE Proc. Circ. Devices Syst. (2003). https://doi.org/10.1049/ip-cds:20030556
7. R. Çapan, A.K. Ray, A.K. Hassan, Thin Solid Films (2007). https://doi.org/10.1016/j.tsf.2006.10.107
8. V.P. Egorova, H.V. Grushevskaya, A.S. Babenka, R.F. Chakukov, N.G. Krylova, I.V. Lipnevich, E.V. Vaskovtsev, Semiconductors (2020). https://doi.org/10.1134/S1063782620140092
9. M.F. Mabrook, A.K. Ray, J. Electron. Mater. (2017). https://doi.org/10.1007/s11664-016-5139-4
10. R. Çapan, A.K. Ray, J. Electron. Mater. (2017). https://doi.org/10.1007/s11664-017-5670-y
11. A.K. Jonscher, J. Phys. D (1999). https://doi.org/10.1088/0022-3727/32/14/201
12. M.M. El-Nahass, H.S. Metwally, H.E.A. El-Sayeda, A.M. Hassanien, Mater. Chem. Phys. (2012). https://doi.org/10.1016/j.matchemphys.2012.01.042
13. A.K. Jonscher, *Universal Relaxation Law* (Chelsea Dielectrics Press, London, 1996).
14. A.K. Roy, A. Singh, K. Kumari, K.A. Nath, A. Prasad, K. Prasad, Int. Scholar. Res. Notices (2012). https://doi.org/10.5402/2012/854831
15. K. Funke, Jump relaxation in solid electrolytes. Prog. Solid State Chem. (1993). https://doi.org/10.1016/0079-6786(93)90002-9

16. A.K. Jonscher, J. Menego, IEEE Trans. Dielectr. Electr. Insult. (2000). https://doi.org/10.1109/94.841825
17. M.M. El-Nahassa, H.S. Metwallya, H.E.A. El-Sayeda, A.M. Hassanien, Mater. Chem. Phys. (2012). https://doi.org/10.1016/j.matchemphys.2012.01.042
18. A.A. Dakhel, Chem. Phys. Lett. (2004). https://doi.org/10.1016/j.cplett.2004.06.094
19. K.H. Mahmoud, F.M. Abdel-Rahim, K. Atef, Y.B. Saddeek, Curr. Appl. Phys. (2011). https://doi.org/10.1016/j.cap.2010.06.018
20. Y.B. Taher, A. Oueslati, N.K. Maaloul, K. Khirouni, M. Gargouri, Appl. Phys. A (2015). https://doi.org/10.1007/s10876-015-0865-y
21. Z.G. Özdemir, M. Kılıç, Y. Karabul, B.S. Mısırlıoğlu, Ö.A. Çataltepe, O. İçelli, Mater. Sci. Semiconductor Proc. (2017). https://doi.org/10.1016/j.mssp.2017.02.020
22. A.R.M. Yusoff, W.H.A. Majid, Eur. Phys. J. B (2005). https://doi.org/10.1140/epjb/e2005-00161-0
23. K.A. Verkhovskaya, A.S. Ievlev, A.M. Lotonov, N.D. Gavrilova, V.M. Fridkin, Phys. B (2005). https://doi.org/10.1016/j.physb.2005.07.003
24. W.H. Abd. Majid, Pyroelectric activity in cyclic and linear polysiloxane Langmuir-Blodgett films PhD Thesis (Sheffield University 1994)